Comprehensive identification of plasma membrane repair proteins revealed spatiotemporal cellular responses to plasma membrane damage

Yuta Yamazaki[1] and Keiko Kono[1]*

1 Okinawa Institute of Science and Technology Graduate University, 1919-1 Tancha, Onna, Okinawa, 904-0495, Japan
* Corresponding author. E-mail: keiko.kono@oist.jp (K.K.)

Abstract

Damage to the plasma membrane (PM) is common in all types of cells. PM repair processes, including exocytosis and endocytosis, are not mutually exclusive; rather, they collaborate to repair the wound. However, the temporal coordination between the repair processes remains poorly understood. Here, by comprehensively identifying PM repair proteins, we resolved the temporal PM repair processes at the damage site in *Saccharomyces cerevisiae*. Of the 80 repair proteins identified, 72 proteins were previously unreported repair protein candidates. We showed that polarity establishment, polarized exocytosis, and clathrin-mediated endocytosis (CME) occur in a specific temporal order at the damage site. Furthermore, we showed that polarized exocytosis and CME are coupled at the damage site, delivering PM repair proteins with transmembrane domains between the growing bud site and the damage site. This study provides insights into the temporal dynamics of coordinated cellular response to PM damage.

MAIN TEXT

Introduction

The plasma membrane (PM) functions as a defensive barrier in all types of cells to protect cellular components from extracellular stimuli. PM frequently experiences physiological and pathological damages, such as eccentric contraction-induced injuries, migration-induced injuries, pore formation by bacterial toxins, or invasion by cancer cells (1, 2). Cells undergo cell lysis if damaged PM is not repaired. Deficits in PM repair are linked to multiple diseases, including limb-girdle muscular dystrophy (3) and Scott syndrome (4, 5). Therefore, virtually all cells have PM repair machinery.

In eukaryotes, the influx of Ca^{2+} triggers PM repair (*1*). Upon Ca^{2+} influx, fundamental cellular mechanisms, including exocytosis (*6-10*), endocytosis (*11, 12*), membrane shedding by ESCRT complex (*13, 14*), and the constriction forces by actin cytoskeleton (*15-18*) are directed to the damage site to reseal the wound. These initial repair processes usually occur within 1 min after PM damage (*19*). After the resealing of the damaged PM, cells restructure the damaged PM (*19, 20*). Restructuring is defined as the process by which cells modify the damaged PM to restore PM homeostasis and normal cell function (*19, 20*). These repair processes are not mutually exclusive, and they collaborate to repair the damaged PM (*21*). However, the temporal coordination between the PM repair processes remains poorly understood.

Both resealing and restructuring of the damaged PM are mediated by the proteins, which accumulate at the damage site. Here, we defined them as PM repair proteins. PM repair proteins include ESCRT, annexins, and dysferlin in mammalian cells (*13, 22-24*). Using budding yeast *Saccharomyces cerevisiae* as a model, we previously identified evolutionarily conserved repair proteins, including protein kinase C, exocyst, and phospholipid flippases (*25, 26*). These repair proteins accumulate at the damage site at the appropriate time and proceed with the repair processes. Therefore, obtaining proteome changes over time at the damage site is an important step toward understanding the temporal PM repair processes.

Here, we performed proteome-scale screening of PM repair proteins using yeast GFP-tagged libraries and laser-induced injury assay in budding yeast. We identified 80 repair protein candidates, including 72 previously unreported candidates. The live-cell imaging of GFP-tagged PM repair proteins revealed the order of repair protein recruitments at the damage site. Among the observed repair processes, we showed that polarized exocytosis and clathrin-mediated endocytosis (CME) are coupled at the damage site, with exocytosis predominating in the early stage of PM repair and CME predominating in the late stage of PM repair. They deliver repair proteins with transmembrane domains (TMDs) between the growing bud site (bud tip) and the damage site, presumably contributing to the restructuring of the damaged PM and to growth resumption after repair. These results provide insights into the temporal dynamics of coordinated cellular responses to PM damage.

Results

Proteome-scale identification of PM/cell wall damage-responsive proteins

To identify the PM repair proteins, we performed a two-step screening. First, we identified the proteins that change localization in response to SDS treatment, which induces local PM/cell wall damage to budding yeast (*27*). We used a yeast C-terminally GFP-tagged library (4159 ORFs) (*28*) and a N-terminally sfGFP-tagged library (N' Swat library) (5569 ORFs) (*29*) comprising 86% of yeast proteome (5718 ORFs in total) (Fig. 1A). We fixed the cells with paraformaldehyde after 1 hour of SDS treatment, in which condition the best-characterized repair protein Pkc1-GFP changes its localization (Fig. 1A). We successfully imaged the signal of 9181 proteins fused with GFP or sfGFP (5609 ORFs in total). We assessed the localization changes of 5609 proteins by visual inspection of the images and identified 562 proteins whose localization changed after SDS treatment (Fig. 1B). In addition to Pkc1, we identified previously reported repair proteins, such as

Dnf1 and Myo2, as screening hits (*25, 26*) (Data S1). Gene Ontology (GO) analysis of the screening hits revealed significant enrichment for proteins involved in the cell polarity establishment process (Fig. 1C). This is consistent with the previous study that SDS treatment remodels the cell polarity and actin cytoskeleton (*25*). Based on the subcellular localization, we categorized the screening hits into six major classes and several minor ones representing less than ten proteins (Fig. 1D and fig. S1, see Materials and Methods). Some proteins that localized to the cell periphery showed cytoplasmic dots after SDS treatment (Fig. 1D). This is consistent with the fact that endocytosis of PM proteins contributes to cell adaptation to environmental stress (*30*). We also found that proteins that form puncta/foci after the SDS treatment include translation factor Gcd7-GFP (Fig. 1D), which forms foci in response to glucose deprivation (*31*). These observations suggest that SDS treatment induces stress responses, including those associated with PM/cell wall damage responses in budding yeast.

Laser-induced PM/cell wall damage assay identified 80 repair protein candidates

Our group previously developed a laser-induced PM/cell wall injury assay under live single-cell conditions (laser damage assay) (*25, 32*). We performed the laser damage assay to identify the PM repair proteins and observe their spatiotemporal movements after PM/cell wall damage (Fig. 2A). The N-terminally sfGFP-tagged library is expressed under exogenous *NOP1* promoters, while the C-terminally GFP-tagged library is expressed under endogenous promoters (*28, 29*). To assess the proteins with endogenous expression levels, we selected the 234 screening hits from the C-terminal library as targets for the laser damage assay. During 25 min of observation at 30-second intervals, we identified 90 proteins whose localization changed in response to laser damage (Fig. 2B). We categorized the proteins into four classes based on their localization changes (Fig. 2C). Three of the puncta-forming proteins, Dna2, Dot6, and Gcd7, form puncta in response to cellular stresses (*31, 33*). In addition, the transcription factors, Msn2 and Crz1, translocate from the cytoplasm to the nucleus after laser damage (Fig. 2B). Msn2 and Crz1 are activated under various stress conditions (*34*). Thus, the localization changes of puncta-forming proteins and transcriptional factors suggest common stress responses to laser damage and other cellular stresses. The most frequently observed localization changes were the accumulation at the damage site (Fig. 2B). We defined them as repair protein candidates, given their presumed involvement in the PM/cell wall repair process.

To gain further insight into the repair protein candidates, we classified them into four categories based on their subcellular localization (Fig. 2C). The largest category is bud-localized proteins (47 proteins) (Fig. 2C), which is consistent with a previous study that bud-localized proteins accumulate at the damage site in budding yeast (*25*). The repair protein candidates in this category include ten proteins that have transmembrane domains (TMDs), including phospholipid flippases (Dnf1/Dnf2) and osmosensor proteins (Slg1, Sho1) (Fig. 2C). Proteins with TMDs are transported to the PM as cargoes of secretory vesicles (*35*). Thus, this result suggests that secretory vesicles targeted to the damage site provide repair proteins with TMDs to the damage site. The second largest category is actin-localized proteins (25 proteins). This is consistent with the GO analysis that actin-binding proteins and proteins involved in actin-related biological processes are enriched in the repair protein candidates (Fig. 2, D and E). The proteins in this category include endocytic proteins, suggesting that endocytosis occurs at the damage site. In addition, proteins that bind actin cables, such as Abp140, are included in this category, suggesting that actin cables are formed at the damage site. These results are consistent with previous studies of PM damage repair in budding yeast and human cells (*11, 25*).

The order of repair protein recruitments at the damage site

Although previous studies have identified and characterized repair proteins, including ESCRT and annexins (*13, 22, 23*), our understanding of the order of the repair processes at the damage

site remains incomplete. The order of repair processes may be linked to the order of repair protein recruitments. Therefore, we investigated the order of repair protein recruitments by quantifying the fluorescence intensity at the damage site over time. We defined accumulation time as the time when the fluorescence intensity at the damage site exceeded the threefold standard deviation (3xSD) above the non-damaged site for at least two consecutive time frames (1 min). We also defined dispersion time when the fluorescence intensity at the damage site becomes less than that of the non-damaged site plus 3xSD for at least 1 min. The bar plot from the accumulation time to the dispersion time provides a visual representation of the order of repair protein recruitments (Fig. 3A). The plot showed that the proteins involved in polarity regulation (Ack1, Msb1, Pkc1, and Bud6) accumulated earlier than exocyst (Sec5, Exo84) and exocytic cargoes with TMD (Dnf1/Dnf2, Slg1, etc.) (Fig. 3A). Consistent with these results, the laser damage assay demonstrated that the Pkc1-sfGFP accumulated at the damage site earlier than Dnf1-mSc-I (Fig. S2). These results suggest that polarity establishment at the damage site is one of the earliest processes observed here in budding yeast.

We found that the proteins involved in clathrin-mediated endocytosis (CME) showed diverse accumulation times (Fig. 3A and fig. S3A). The CME markers, Sla1-GFP and Abp1-GFP (*36*), exhibited repeated short stays and reaccumulation at the damage site within 5 min to 25 min after laser damage (Fig. S3, B to D). In contrast, Dnf1-GFP showed stable accumulation at the damage site (Fig. S3E). These results suggest that CME repeatedly occurs at the damage site within a relatively short time frame. Given that exocytic cargoes (Dnf1, Dnf2, Sho1) and exocyst subunits (Sec5, Exo84) accumulate at the damage site within 5 min after laser damage (Fig. 3A), we hypothesize that exocytosis and CME occur simultaneously at the damage site. To test this idea, we performed the laser damage assay in the cells expressing Exo70-mNG/Dnf1-mNG and Ede1-mSc-I (Fig. 3, B and C). Ede1 is one of the earliest proteins recruited to endocytic sites, serving as a CME marker (*37*, *38*). Exo70 is one of the subunits of the exocyst complex, serving as an exocytosis marker. Exo70-mNG/Dnf1-mNG and Ede1-mSc-I simultaneously accumulated at the damage site from 5 min to 35 min (Fig. 3, B and C). The signals of Exo70-mNG/Dnf1-mNG peak around 10 min after the damage, while Ede1-mSc-I peaks 20 min after the damage (Fig. 3, B and C). These results suggest that CME and exocytosis occur simultaneously at the damage site, with exocytosis predominating in the early stage of the PM/cell wall damage response and CME predominating in the late stage of the PM/cell wall damage response.

Knockout mutants of CME are sensitive to PM/cell wall stresses

To identify the biological processes required for cell survival after PM/cell wall stress, we performed growth screening of repair protein knockout mutants in PM/cell wall stress conditions (Fig. S4A). We spotted the same number of yeast cells in YPD media, YPD+0.01% SDS media, YPD+25 μg/ml calcofluor white (CFW), and YPD media in 37 ℃ (Heat stress) and incubated for 3 days (Fig. S4A). CFW binds to chitin in the cell wall, inducing cell wall damage (*39*). Heat stress modifies PM structures (*40*). The growth assay showed that six knockout mutants of CME proteins, *rvs167*Δ, *sla1*Δ, *sla2*Δ, *end3*Δ, *las17*Δ, and *vrp1*Δ, are sensitive to all the stress conditions (Fig. S4B). We knocked out these genes using the WT strain in our laboratory and confirmed that these mutants are sensitive to SDS (Fig. S4C). These results led us to focus further on the CME functions associated with PM/cell wall damage repair.

CME proteins are required for polarized exocytosis and actin cable organization at the damage site

Previous studies showed that endocytosis is involved in PM damage repair by directly resealing the PM by removing the damaged pores (*41*) or by restructuring the PM after resealing in mammalian cells (*20*, *42*). We showed that CME occurs at the damage site from 5 to 45 min after laser damage in budding yeast (Fig. 3, A to C, and fig. S3, B and C). This supports the possibility

that CME restructures the PM after resealing, which usually occurs within 1 min after the damage (*20*). Another potential mechanism for restructuring the damaged PM is exocytosis, which delivers PM proteins and lipids to the damage site. Given that CME and polarized exocytosis constitute a coupled transport cycle in budding yeast (*43*), we reasoned that CME positively regulates exocytosis at the damage site, thereby restructuring the damaged PM.
To test this idea, we performed the laser damage assay in SDS-sensitive endocytic mutants (*sla1*Δ, *end3*Δ, *vrp1*Δ, and *rvs167*Δ). We used two exocytosis markers, type V myosin (Myo2) and the exocyst subunit (Exo70), fused to sfGFP and mNG, to assess the exocytosis activity at the damage site. The accumulation of Myo2-sfGFP and Exo70-mNG at the damage site was impaired in *sla1*Δ, *end3*Δ, and *vrp1*Δ (Fig. 4, A and B, fig. S5, A and B). The observed weak phenotype of *rvs167*Δ for the accumulation of Myo2-sfGFP and Exo70-mNG is consistent with the previous study that exocytosis is not impaired in *rvs167*Δ (*43*). Myo2 transports secretory vesicles and the exocyst complex to the polarized sites along with actin cables (*44*). We, therefore, hypothesized that CME proteins contribute to the actin cable organization at the damage site. To visualize actin cables, we expressed Abp140-GFP, which marks actin cables (*45*). The accumulation of Abp140-GFP at the damage site suggests the formation of actin cables at the damage site (Fig. 4C). In *sla1*Δ, *end3*Δ, and *vrp1*Δ, the accumulation of Abp140-GFP at the damage site was impaired (Fig. 4C and fig. S5C). These results suggest that CME proteins are required for polarized exocytosis and actin cable organization at the damage site.

CME at the bud tip directs repair proteins to the damage site

Although the requirement of Rvs167 for actin cable organization and exocytosis at the damage site is minimal (Fig. 4, A to C), *rvs167*Δ is sensitive to SDS (Fig. S4C). This raised the possibility that CME plays additional roles, such as membrane protein trafficking, in PM repair. We found that CME proteins, including Apl1, Ede1, and Ent1, changed their localization from the bud neck to the bud tip within 10 min after laser damage (Fig. 5A). The fluorescence intensity changes of CME proteins at the bud tip were significantly higher than those of other repair protein candidates (Fig. 5B and fig. S6, A and B). Consistent with these results, the Ede1-mSc-I signal at the bud tip increased within 10 min after laser damage (Fig. 5C). These results suggest that CME occurs at the bud tip within 10 min after laser damage. We also found that Dnf1-mNG disappeared from the bud tip following the recruitment of Ede1-mSc-I to the bud tip (Fig. 5, C and D). The disappearance from the bud tip and the accumulation at the damage site of Dnf1-mNG were impaired in *rvs167*Δ (Fig. 5, D and E, and fig. S7). Furthermore, the disappearance from the bud tip and the accumulation at the damage site of repair proteins with TMDs (Slg1-sfGFP and Sho1-GFP) and representative endocytic recycling cargo, mNG-Snc1 were impaired in *rvs167*Δ (Fig. 5, F to H and fig. S8, A to C). These results support our idea that CME directs repair proteins with TMD from the bud tip to the damage site, thereby restructuring the damaged PM.

mNG-Snc1 is retargeted from the damage site to the bud tip

The fluorescence intensity of accumulated repair proteins with TMDs at the damage site gradually decreases approximately 15 min after laser damage (Fig. 3, B and C, and fig. S8, A-C). As CME persistently occurs at the damage site from 5 to 45 min after laser damage (Fig. 3, A to C, and fig. S3, B and C), accumulated CME cargoes are likely to be endocytosed. We hypothesized that endocytosed CME cargoes are retargeted to the bud tip after PM repair. We test this possibility using mNG-Snc1 as a model. To exclude the possibility that newly synthesized mNG-Snc1 is transported to the bud tip, we transiently expressed mNG-Snc1 under the control of the galactose-inducible promoter (Gal1pr) for 1 hour (Fig. 6A). Then, we transferred the cells to glucose media to stop the expression (Fig. 6A). To minimize the effect of changing the carbon source, we further incubated the cells in glucose media for at least 3 hours prior to laser damage (Fig. 6A). The mNG-Snc1 accumulated at the damage site approximately ~10 min after laser damage, gradually

disappearing after the colocalization with Ede1-mSc-I (Fig. 6A and B). The mNG-Snc1 signal at the bud tip decreased to 10-40% ~20 min after laser damage (Fig. 6C and D). Around 30 min to 60 min after laser damage, the normalized mNG-Snc1 signal at the bud tip recovered to 65-89% (Fig. 6, C and D). These results suggest that mNG-Snc1 is redirected to the bud tip after PM repair, presumably via CME at the damage site. We propose that CME at the damage site retarget the accumulated repair proteins with TMDs from the damage site to the bud tip, allowing the cell to resume growth after PM repair.

Discussion

There has been a growing interest in the mechanisms underlying PM repair, partly due to their association with human diseases and cellular aging (*3-5, 27*). PM repair proteins, which accumulate at the damage site, play critical roles in PM repair. In this study, we comprehensively identified PM repair proteins and defined the spatiotemporal PM repair processes in budding yeast (Fig. 7).

By combining proteome-scale visual screening using yeast GFP libraries and the laser damage assay, we identified 80 repair protein candidates (Fig. 2B). The proteins involved in polarity establishment and endocytosis are enriched in the repair protein candidates (Fig. 2E), consistent with previous studies in budding yeast and human cells (*11, 25*). Strikingly, 72 out of 80 repair protein candidates were not previously reported to accumulate at the damage site in budding yeast (*25, 26*). The unreported repair protein candidates include uncharacterized proteins, such as Sap1 and Ypr089w (Fig. 3A and Data S2). Characterizing these proteins may expand our understanding of PM repair mechanisms.

We selected the screening hits from the C-terminally GFP-tagged library as targets for the laser damage assay. Although this is a reasonable approach to evaluating the proteins from the endogenous expression level, it overlooks the potential repair proteins in the N-terminally sfGFP-tagged library. For example, sfGFP-Snc2, but not Snc2-GFP, changes localization in response to SDS treatment because of the mislocalization of Snc2-GFP in the vacuole. Because Snc2 is a homolog of Snc1, Snc2 is a potential repair protein. Screening hits from the N-terminally sfGFP-tagged library can also be a useful resource for further repair protein identification.

It should be noted that this screening is unable to identify proteins whose localization remains unaltered in response to SDS treatment. For example, we could not identify Cdc50-Drs2, which accumulates at the damage site induced by a laser (*26*). A recent study demonstrated the different cellular responses between focal (laser damage) and diffuse (streptolysin-O (SLO) treatment) PM damages (*6*). Some proteins may be overlooked in the screening due to the intrinsic differences between SDS treatment and the laser damage assay. In addition, the screening did not identify ESCRT proteins as hits. The tagging of fluorescent proteins occasionally interferes with the functions of the tagged proteins (*46*). Specifically, the exogenous expression of fluorescent-tagged ESCRT subunits can impair their functions (*47, 48*). The screening may have overlooked some of these proteins, possibly including ESCRT proteins.

By quantifying the fluorescence intensity at the damage site over time, we report the order of repair protein recruitments at the damage site, which may be linked to the order of repair processes. Among them, Ack1-GFP and Msb1-GFP are the earliest proteins to accumulate at the damage site. Ack1 and Msb1 function as activators of the Rho1-Pkc1 pathway (*49, 50*). The accumulation times of Ack1-GFP, Msb1-GFP, and Pkc1-GFP are 0.5, 0.5, and 1 min, respectively. Thus, Rho1-Pkc1 pathways may be involved in the initial repair processes, such as the resealing of the damaged PM.

We demonstrated that polarized exocytosis and CME occur simultaneously at the damage site between approximately 5 to 35 min after laser damage (Fig. 3). Given that the resealing of the damaged PM generally occurs within 1 min (*20*), this result implied that exocytosis and

endocytosis are involved in the restructuring of the damaged PM rather than the resealing of it. The coupling of endocytosis with polarized exocytosis is observed in multiple cell types, including at the growing tip of budding yeast, the growing tip of pollen tubes, and synapses in neurons (*51*). Exocytosis and endocytosis at the damage site may regulate the PM tensions and amount of lipids and PM proteins in a manner analogous to that observed in these cells. Interestingly, our results suggest that the activity of CME and polarized exocytosis at the damage site changes over time, with exocytosis predominating within 20 min after laser damage and CME predominating 20 min after laser damage. (Fig. 3, B and C). A previous study showed that polarized exocytosis activates CME in budding yeast (*43*). Rab GTPase Sec4, which regulates polarized exocytosis, also activates endocytosis by overriding Sla1 inhibition of Las17 (*43*). We could not identify Sec4 as a repair protein candidate because C-terminally GFP-tagged Sec4 is not in the library, probably due to the loss of functions of C-terminally tagged Sec4. However, we found that Sec2-GFP, the guanine nucleotide exchange factor (GEF) of Sec4, accumulates at the damage site within 5 min after laser damage (Fig. 3A and Data S2). Sec4 and Sec2 localize to the secretory vesicles (*52, 53*). Therefore, secretory vesicles that are targeted to the damage site may accumulate Sec2 and Sec4, leading to the activation of CME. The switching of activities between exocytosis and CME may contribute to restoring PM homeostasis after the damage.

Among the repair protein candidates, CME proteins are required for yeast growth in PM/cell wall-damaging conditions (Fig. S4). Although endocytosis has been reported to be involved in PM repair, previous studies focused on their functions in removing the damaged PM (*11, 12, 20*). Here, we showed that CME delivers repair proteins with TMDs between the bud tip and the damage site (Fig. 7).

Polarized exocytosis and actin cable organization at the damage site are inhibited in CME mutants (Fig. 4). Given that exocytic vesicles are transported along with actin cables (*44*), the observed impairment in exocytosis may be attributed to the impaired organization of actin cables at the damage site. CME proteins, including Sla1, End3, and Vrp1, are involved in actin polymerization, which results in the formation of cortical actin patches (*54, 55*). ADP-actin in cortical actin patches may be recycled for actin cable formation (*56*), raising the possibility that CME at the damage site contributes to actin cable formation by providing actin monomers. Alternatively, the recruitment of polarity regulators, including Rho1 and Cdc42, to the damage site might be inhibited in CME mutants. These possibilities should be further investigated in the future.

Previous studies showed that endocytosis actively occurs at the damage site to repair the damaged PM (*11, 12, 20*). Surprisingly, our results suggest that CME actively occurs at the bud tip within 10 min after laser damage. In *rvs167*Δ, in which exocytosis inhibition at the damage site is minimal (Fig. 4), repair proteins with TMDs at the bud tip fail to accumulate at the damage site (Fig. 5). These results are consistent with our idea that CME at the bud tip directs repair proteins with TMDs to the damage site (Fig. 7). Consistent with our results, dysferlin-containing vesicles increase in response to PM damage in muscle cells (*24, 57*). Dysferlin has a TMD and functions as a PM repair protein (*24, 57, 58*). Delivery of repair proteins with TMDs from non-damaged sites to the damage site by endocytosis may occur in a wide range of eukaryotic species.

We showed that 65-89% of normalized mNG-Snc1 signal at the bud tip is recovered approximately 40 min after the damage (Fig. 6, C and D). Because Snc1 is a CME cargo and it colocalizes with Ede1-mSc-I at the damage site, it is presumably recovered from the damage site via CME. A previous study showed that macropinocytosis restructures the damaged PM in human cells (*20*). However, it is not clear whether the cargo proteins are recycled or degraded. We propose that CME terminates the PM damage response by removing the repair proteins with TMDs from the damage site and resuming the growth by retargeting them to the bud tip (Fig. 7).

In summary, our two-step visual screening reveals spatiotemporal events occurring after PM damage. Despite the limitations mentioned above, our screening provides the first functional catalog of repair proteins and insights into the temporal dynamics of coordinated cellular

responses to PM damage. Because some of the PM repair protein candidates identified in this study and CME mechanisms are evolutionarily conserved, this work may serve as a basis for future studies, including those to be conducted in mammalian cells.

Materials and Methods

Media and strains

Standard procedures were used for DNA manipulations, *E. coli*, and yeast genetic manipulations. Yeast transformations were performed using the lithium acetate method. A PCR-based procedure was used for gene deletion. The deletion of the expected locus was confirmed by colony PCR (*59*). Yeast cells were cultured in YPD media (1% yeast extract, 2% bacto peptone, and 2% glucose) unless otherwise indicated. SD media (yeast nitrogen base (6.7 g/liter) without amino acids, L-adenine (550 mg/liter), L-arginine (280 mg/liter), L-alanine (280 mg/liter), L-asparagine (280 mg/liter), L-aspartic acids (280 mg/liter), L-cysteine (280 mg/liter), glycine (280 mg/liter), L–glutamic acids (280 mg/liter), L-glutamine (280 mg/liter), L-isoleucine (280 mg/liter), L-lysine (280 mg/liter), L-phenylalanine (280 mg/liter), L-proline (280 mg/liter), L-serine (280 mg/liter), L-threonine (280 mg/liter), L-tyrosine (280 mg/liter), L-valine (280 mg/liter), leucine (530 mg/liter), methionine (86 mg/liter), histidine (86 mg/liter), uracil (22 mg/liter), myo-inositol (100 mg/liter), and *p*-aminobenzoic acid (3 mg/liter) (pH 5.5)) were used for laser damage assay. Yeast culture was performed at 25°C unless otherwise indicated. The yeast strains, yeast libraries, and plasmids used in this study are listed in Tables S1 to S3.

For the mNG-Snc1 expression experiments in Fig. 6, we grow cells in SD media containing 2% raffinose instead of glucose overnight. Then, we induced the expression of mNG-Snc1 by adding 3% galactose. After one hour of growth in galactose media, the cells were centrifuged at 5000xg for 5 min, and the spun-down cells were washed twice with SD media containing 2% glucose. We transferred the spun-down cells to SD media containing 2% glucose. The cells were incubated for at least 3 hours before the laser damage assay.

GFP screen for SDS damage response

GFP strains were spotted onto the YPD plates from 96-well plates using a pin replicator and incubated at 25℃. After 3 days, the colonies were inoculated into the 200 µl of YPD media and incubated overnight to saturation. After mixing, 3 µl of the saturated culture was transferred to 1 ml of YPD media in deep well plates and grew for 4-5 hours. 500 µl of the cultures were transferred to the new deep well plates. 10 µl of 1% SDS was added to 500 µl of cultures and incubated at 25℃ for 1 hour. The cells were centrifuged at 2000xg for 2 min. The cells were fixed by 300 µl of 4% PFA in YPD for 30 min at room temperature. The fixed cells were centrifuged at 2000xg for 2min. Cells were washed twice with PBS and centrifuged at 2000xg for 2 min. The supernatant was removed between each wash. Cells were kept at 4℃ until imaging. Cells were imaged with an LSM880 confocal microscope using a 20x air objective lens with an airyscan detector for GFP fluorescence (Ex 488/Em522). Maximum intensity projections of z-stack images are shown.

Categorization of localization changes in response to SDS treatment

We manually reviewed the acquired images using Zen Blue edition (Zeiss) or Fiji software (*60*) and compared the localization of GFP-tagged proteins in normal and SDS treatment conditions. We categorized the screening hits based on reported protein localization. We first categorized the bud tip- or the bud neck-localizing proteins as “From bud tip/neck”. Among the uncategorized remaining screening hits, the actin-localizing proteins were categorized as “Actin”. Among the remaining uncategorized screening hits, cell periphery-localizing proteins were categorized as “From cell periphery.” Among the remaining uncategorized screening hits, nucleus-localizing

proteins were categorized as “Nucleus” or “Nucleus to the cytoplasm”. We categorized Urc1 as “Nucleus to cytoplasm” because its signal dispersed to the cytoplasm in an SDS treatment condition. Other proteins in the “Nucleus” showed stronger nucleus localization in the SDS treatment conditions. Among the remaining uncategorized screening hits, we categorized mitochondria-localizing proteins as “Mitochondria”. Among the remaining uncategorized screening hits, we categorized spindle pole-localizing proteins as “Spindle pole.” All proteins in the “Spindle pole” showed stronger dot-like structures in the SDS treatment condition. Among the remaining uncategorized screening hits, we categorized proteins that show puncta or foci in SDS treatment conditions as “Puncta/foci.” We categorized Gcn2, Ato3, Sun4, Csi2, Sps4, and Ypr089w as “Puncta/foci dispersed” because they showed weaker foci or puncta signals in SDS treatment conditions. We categorized Tul1, Emp24, Hor7, Scw10, and Ynl019c as “From vacuole” because they showed decreased vacuole signal in the SDS treatment conditions. We categorized Prm5 as “to vacuole” because its vacuole signal increases. We categorized Yps1 and Msc1 as “cytoplasm to ER” because they localize to ER, and their ER signal increased in SDS treatment conditions. In this study, we make use of the protein localization data from the Saccharomyces Genome Database (SGD) and (*28*). All results of this screening are shown in Data S1.

Laser damage assay

Yeast cells were grown in SD medium at 25°C until the culture reached an OD600 of 0.1-0.4. We diluted the yeast culture and further incubated yeast cells in SD medium for 3-8 hours at 25˚C. We took 1 mL of the culture and centrifuged it at 500xg for 5 min to spin the cells down. We took 5-10 µL of the cell suspension and placed it onto SD medium + 2.2% agarose bed. A Concanavalin A (ConA) (Nacalai Tesque) coated glass slip was placed on the cells prior to imaging.

Cells were observed with A1R (Nikon). A1R was equipped with a CFI Apochromat TIRF 60×/1.49 oil objective lens (Nikon). GFP, mNG, and sfGFP were excited by a 488 nm laser, and the fluorescence that passed a 525/50 nm band-pass filter was detected with a GaAsP detector. mSc-I was excited by a 561 nm laser, and the fluorescence that passed a 595/50 nm band-pass filter was detected with a GaAsP detector. For laser damage assays, the 405 nm laser was irradiated to a circle of 0.5 µm diameter in a cell periphery. The laser power was set between 30% to 70% depending on the fluorescence-tagged proteins. We set the laser power so that it does not rupture the yeast cells. To compare the accumulation of proteins between mutants, we set the exact same laser power and microscopy setting between mutants.

Categorization of localization changes in response to laser damage

We categorized proteins that accumulate at the damage site as “Damage site”. These proteins are defined as repair protein candidates. Among the remaining uncategorized proteins, we categorized cell periphery-localizing proteins as “PM to cytoplasm”. Among the remaining uncategorized proteins, we categorized Msn2 and Crz1 as "Nucleus" because they changed localization from the cytoplasm to the nucleus. Among the remaining uncategorized proteins, we categorized Dot6, Dna2, Msc1, and Gcd7 as "Puncta" because they formed punctate structures in response to laser damage. The repair protein candidates identified in this study are listed in Data S2.

Quantification of fluorescence signal for laser damage assay

The quantification of the fluorescence signal from the laser damage assay was performed as described previously (*26*). For the comprehensive identification of repair protein candidates, we selected the region of interest (ROI) around the whole cell, the damage site, and the bud tip of the cells. We manually move the ROIs as the cell moves so that the ROIs remain at the same position in the cell. At least three cells are measured for quantification. We used the ROIs with the

maximum mean fluorescence intensity for quantification. For other laser damage assays, we set the ROIs and manually selected them for quantification. The fluorescence intensity at the damage site and the bud tip were normalized by the fluorescence intensity of a whole cell to minimize the effect of photobleaching during imaging.

In Fig. 3A, we defined the accumulation time as the time when the fluorescence intensity at the damaged site became greater than the fluorescence intensity at the non-damaged site by 3× standard deviation (3xSD) for at least two consecutive time frames. We defined dispersion time when the fluorescence intensity at the damage site becomes less than that of the non-damaged site plus 3xSD for at least two consecutive time frames after accumulation time. We measured at least three cells. The median values of accumulation times and dispersion times across replicates are presented. The accumulation time and dispersion time of all repair protein candidates are listed in Data S2.

Growth screening of repair protein knockout mutants

Yeast cultures grown overnight in YPD at 25°C were diluted to OD600 = 0.1. The diluted cultures were spotted onto YPD, YPD + 0.01% SDS, and YPD + 25 μg/ml CFW plates. After 3 days of incubation at 25°C or 37°C (Heat stress), the growth of the YPD plate and other plates were compared. We performed the screening of two independent colonies. The strains were from the yeast deletion collection library (*61*) except for *smi1*Δ, *las17*Δ, *skg6*Δ, *end3*Δ, *vrp1*Δ, and *sla2*Δ. Only the mutants that showed sensitivity to the stress in two independent colonies were defined as sensitive to the stress. The results of the screening are shown in Data S2.

Spot assay

Yeast cultures grown overnight in YPD at 25°C were diluted to OD600 = 0.1. The four-fold serial dilutions of cultures were spotted onto the indicated plates.

Statistical Analysis

Dunnett's multiple comparison test, Welch's t-test, and Mann–Whitney U test were performed with Python software (v. 3.11). Gene enrichment analysis and Fisher's exact test were performed with R software (v. 4.2.2).

References

1. P. L. McNeil, T. Kirchhausen, An emergency response team for membrane repair. *Nature reviews. Molecular cell biology* **6**, 499-505 (2005).
2. C. Dias, J. Nylandsted, Plasma membrane integrity in health and disease: significance and therapeutic potential. *Cell Discov* **7**, 4 (2021).
3. R. Bashir *et al.*, A gene related to Caenorhabditis elegans spermatogenesis factor fer-1 is mutated in limb-girdle muscular dystrophy type 2B. *Nat Genet* **20**, 37-42 (1998).
4. J. Suzuki, M. Umeda, P. J. Sims, S. Nagata, Calcium-dependent phospholipid scrambling by TMEM16F. *Nature* **468**, 834-838 (2010).
5. N. Wu *et al.*, Critical Role of Lipid Scramblase TMEM16F in Phosphatidylserine Exposure and Repair of Plasma Membrane after Pore Formation. *Cell reports* **30**, 1129-1140 e1125 (2020).
6. D. C. Bittel, J. K. Jaiswal, Early Endosomes Undergo Calcium‐Triggered Exocytosis and Enable Repair of Diffuse and Focal Plasma Membrane Injury. *Advanced Science* **10**, (2023).
7. N. Raj *et al.*, Early Endosomes Act as Local Exocytosis Hubs to Repair Endothelial Membrane Damage. *Advanced Science* **10**, 2300244 (2023).
8. A. Reddy, E. V. Caler, N. W. Andrews, Plasma Membrane Repair Is Mediated by Ca2+-Regulated Exocytosis of Lysosomes. *Cell* **106**, 157-169 (2001).
9. G. Q. Bi, J. M. Alderton, R. A. Steinhardt, Calcium-regulated exocytosis is required for cell membrane resealing. *Journal of Cell Biology* **131**, 1747-1758 (1995).
10. K. Miyake, P. L. McNeil, Vesicle accumulation and exocytosis at sites of plasma membrane disruption. *Journal of Cell Biology* **131**, 1737-1745 (1995).
11. V. Idone *et al.*, Repair of injured plasma membrane by rapid Ca2+-dependent endocytosis. *The Journal of Cell Biology* **180**, 905-914 (2008).
12. C. Tam *et al.*, Exocytosis of acid sphingomyelinase by wounded cells promotes endocytosis and plasma membrane repair. *J Cell Biol* **189**, 1027-1038 (2010).
13. A. J. Jimenez *et al.*, ESCRT Machinery Is Required for Plasma Membrane Repair. **343**, 1247136 (2014).
14. L. L. Scheffer *et al.*, Mechanism of Ca2+-triggered ESCRT assembly and regulation of cell membrane repair. *Nature Communications* **5**, 5646 (2014).
15. C. A. Mandato, W. M. Bement, Actomyosin transports microtubules and microtubules control actomyosin recruitment during Xenopus oocyte wound healing. *Curr Biol* **13**, 1096-1105 (2003).
16. W. M. Bement , H. l. n. A. Benink , G. von Dassow A microtubule-dependent zone of active RhoA during cleavage plane specification. *Journal of Cell Biology* **170**, 91-101 (2005).
17. M. T. Abreu-Blanco, J. M. Verboon, S. M. Parkhurst, Cell wound repair in Drosophila occurs through three distinct phases of membrane and cytoskeletal remodeling. *J Cell Biol* **193**, 455-464 (2011).
18. H. A. Benink, W. M. Bement, Concentric zones of active RhoA and Cdc42 around single cell wounds. *J Cell Biol* **168**, 429-439 (2005).
19. M. L. Ebstrup, C. Dias, A. S. B. Heitmann, S. L. Sønder, J. Nylandsted, Actin Cytoskeletal Dynamics in Single-Cell Wound Repair. *Int J Mol Sci* **22**, (2021).
20. S. L. Sønder *et al.*, Restructuring of the plasma membrane upon damage by LC3-associated macropinocytosis. *Science Advances* **7**, eabg1969 (2021).
21. D. A. Ammendolia, W. M. Bement, J. H. Brumell, Plasma membrane integrity: implications for health and disease. *BMC Biology* **19**, (2021).

22. N. J. Lennon *et al.*, Dysferlin Interacts with Annexins A1 and A2 and Mediates Sarcolemmal Wound-healing. *Journal of Biological Chemistry* **278**, 50466-50473 (2003).
23. S. P. Lauritzen, T. L. Boye, J. Nylandsted, Annexins are instrumental for efficient plasma membrane repair in cancer cells. *Semin Cell Dev Biol* **45**, 32-38 (2015).
24. J. R. McDade, A. Archambeau, D. E. Michele, Rapid actin-cytoskeleton-dependent recruitment of plasma membrane-derived dysferlin at wounds is critical for muscle membrane repair. *FASEB journal : official publication of the Federation of American Societies for Experimental Biology* **28**, 3660-3670 (2014).
25. K. Kono, Y. Saeki, S. Yoshida, K. Tanaka, D. Pellman, Proteasomal degradation resolves competition between cell polarization and cellular wound healing. *Cell* **150**, 151-164 (2012).
26. Y. Yamazaki, K. Kono, Clathrin-mediated trafficking of phospholipid flippases is required for local plasma membrane/cell wall damage repair in budding yeast. *Biochemical and biophysical research communications* **606**, 156-162 (2022).
27. K. Suda *et al.*, Plasma membrane damage limits replicative lifespan in yeast and induces premature senescence in human fibroblasts. *Nature Aging* **4**, 319-335 (2024).
28. W.-K. Huh *et al.*, Global analysis of protein localization in budding yeast. *Nature* **425**, 686-691 (2003).
29. I. Yofe *et al.*, One library to make them all: streamlining the creation of yeast libraries via a SWAp-Tag strategy. *Nat Methods* **13**, 371-378 (2016).
30. T. López-Hernández, V. Haucke, T. Maritzen, Endocytosis in the adaptation to cellular stress. *Cell Stress* **4**, 230-247 (2020).
31. S. L. Moon, R. Parker, Analysis of eIF2B bodies and their relationships with stress granules and P-bodies. *Scientific Reports* **8**, (2018).
32. K. Kono, H. Okada, Y. Ohya, Local and Acute Disruption of the Yeast Cell Surface. *Cold Spring Harbor Protocols* **2016**, pdb.prot085266 (2016).
33. J. M. Tkach *et al.*, Dissecting DNA damage response pathways by analysing protein localization and abundance changes during DNA replication stress. *Nature cell biology* **14**, 966-976 (2012).
34. I. Camponeschi, A. Montanari, C. Mazzoni, M. M. Bianchi, Light Stress in Yeasts: Signaling and Responses in Creatures of the Night. *International Journal of Molecular Sciences* **24**, 6929 (2023).
35. Y. Shimizu, T. Uemura, The sorting of cargo proteins in the plant trans-Golgi network. *Frontiers in Plant Science* **13**, (2022).
36. M. Kaksonen, C. P. Toret, D. G. Drubin, A modular design for the clathrin- and actin-mediated endocytosis machinery. *Cell* **123**, 305-320 (2005).
37. R. Lu, D. G. Drubin, Selection and stabilization of endocytic sites by Ede1, a yeast functional homologue of human Eps15. *Molecular biology of the cell* **28**, 567-575 (2017).
38. V. Stradalova *et al.*, Distribution of cortical endoplasmic reticulum determines positioning of endocytic events in yeast plasma membrane. *PLoS One* **7**, e35132 (2012).
39. A. F. J. Ram, A. Wolters, R. T. Hoopen, F. M. Klis, A new approach for isolating cell wall mutants in Saccharomyces cerevisiae by screening for hypersensitivity to calcofluor white. *Yeast* **10**, 1019-1030 (1994).
40. Z. Török *et al.*, Plasma membranes as heat stress sensors: from lipid-controlled molecular switches to therapeutic applications. *Biochim Biophys Acta* **1838**, 1594-1618 (2014).
41. V. Idone *et al.*, Repair of injured plasma membrane by rapid Ca2+-dependent endocytosis. *J Cell Biol* **180**, 905-914 (2008).
42. L. N. Skalman, M. R. Holst, E. Larsson, R. Lundmark, Plasma membrane damage caused by Listeriolysin O is not repaired through endocytosis of the membrane pore. *Biology Open* **7**, bio035287 (2018).

43. J. Johansen, G. Alfaro, C. T. Beh, Polarized Exocytosis Induces Compensatory Endocytosis by Sec4p-Regulated Cortical Actin Polymerization. *PLOS Biology* **14**, e1002534 (2016).
44. K. W. Donovan, A. Bretscher, Myosin-V is activated by binding secretory cargo and released in coordination with Rab/exocyst function. *Developmental cell* **23**, 769-781 (2012).
45. H.-C. Yang, L. A. Pon, Actin cable dynamics in budding yeast. *Proceedings of the National Academy of Sciences* **99**, 751-756 (2002).
46. K. Thorn, Genetically encoded fluorescent tags. *Molecular biology of the cell* **28**, 848-857 (2017).
47. K. Katoh *et al.*, The ALG-2-interacting protein Alix associates with CHMP4b, a human homologue of yeast Snf7 that is involved in multivesicular body sorting. *J Biol Chem* **278**, 39104-39113 (2003).
48. H. K. Hoffman, M. V. Fernandez, N. S. Groves, E. O. Freed, S. B. van Engelenburg, Genomic tagging of endogenous human ESCRT-I complex preserves ESCRT-mediated membrane-remodeling functions. *J Biol Chem* **294**, 16266-16281 (2019).
49. S. A. Krause *et al.*, Functional specialisation of yeast Rho1 GTP exchange factors. *J Cell Sci* **125**, 2721-2731 (2012).
50. Y. Liao, F. He, T. Gong, E. Bi, X.-D. Gao, Msb1 Interacts with Cdc42, Boi1, and Boi2 and May Coordinate Cdc42 and Rho1 Functions during Early Stage of Bud Development in Budding Yeast. *PLoS ONE* **8**, e66321 (2013).
51. V. Gerganova, S. G. Martin, Going with the membrane flow: the impact of polarized secretion on bulk plasma membrane flows. *The FEBS Journal* **290**, 669-676 (2023).
52. N. B. Elkind, C. Walch-Solimena, P. J. Novick, The role of the COOH terminus of Sec2p in the transport of post-Golgi vesicles. *J Cell Biol* **149**, 95-110 (2000).
53. R. M. Gingras, A. M. Sulpizio, J. Park, A. Bretscher, High-resolution secretory timeline from vesicle formation at the Golgi to fusion at the plasma membrane in S. cerevisiae. *Elife* **11**, (2022).
54. R. Lu, D. G. Drubin, Y. Sun, Clathrin-mediated endocytosis in budding yeast at a glance. *Journal of Cell Science* **129**, 1531-1536 (2016).
55. B. L. Goode, J. A. Eskin, B. Wendland, Actin and endocytosis in budding yeast. *Genetics* **199**, 315-358 (2015).
56. D. R. Kovar, E. S. Harris, R. Mahaffy, H. N. Higgs, T. D. Pollard, Control of the Assembly of ATP- and ADP-Actin by Formins and Profilin. *Cell* **124**, 423-435 (2006).
57. J. R. McDade, M. T. Naylor, D. E. Michele, Sarcolemma wounding activates dynamin-dependent endocytosis in striated muscle. *Febs j* **288**, 160-174 (2021).
58. J. Liu *et al.*, Dysferlin, a novel skeletal muscle gene, is mutated in Miyoshi myopathy and limb girdle muscular dystrophy. *Nature Genetics* **20**, 31-36 (1998).
59. M. S. Longtine *et al.*, Additional modules for versatile and economical PCR-based gene deletion and modification in Saccharomyces cerevisiae. *Yeast* **14**, 953-961 (1998).
60. J. Schindelin *et al.*, Fiji: an open-source platform for biological-image analysis. *Nat Methods* **9**, 676-682 (2012).
61. E. A. Winzeler *et al.*, Functional characterization of the S. cerevisiae genome by gene deletion and parallel analysis. *Science (New York, N.Y.)* **285**, 901-906 (1999).
62. A. Krogh, B. Larsson, G. von Heijne, E. L. Sonnhammer, Predicting transmembrane protein topology with a hidden Markov model: application to complete genomes. *J Mol Biol* **305**, 567-580 (2001).

Acknowledgments
We thank Dr. Maya Schuldiner (Weizmann Institute) for providing the N' SWAT library. We thank Dr. S. Sugiyama for providing yeast strains and technical advice. We also thank lab members of the Membranology unit for the discussion and critical reading of the manuscript. We are grateful for the help and support provided by the Imaging Section and Sequence Section of Core Facilities at Okinawa Institute of Science and Technology Graduate University. We thank Dr. P. Barzaghi, Dr. K. Koizumi, Dr. S. Komoto, and Dr. T. Mochizuki for their technical assistance in microscopy experiments.

Funding: This study was supported by MEXT/JSPS KAKENHI Grant Number 23KJ2138 to Y.Y., JSPS grant-in-aid for scientific research (B) Grant Number 20H03440, 24K02233, and JST-COI-NEXT JPMJPF2205 to K.K..

Author contributions:
Conceptualization, Y.Y. and K.K.; Investigation, Y.Y.; Writing – Original Draft, Y.Y.; Writing – Review & Editing, Y.Y. and K.K.; Funding Acquisition, Y.Y. and K.K.; Supervision, K.K**.**

Competing interests: The authors declare that they have no competing interests.

Data and materials availability: All data needed to evaluate the conclusions in the paper are present in the main text and/or the supplementary materials.

Figures

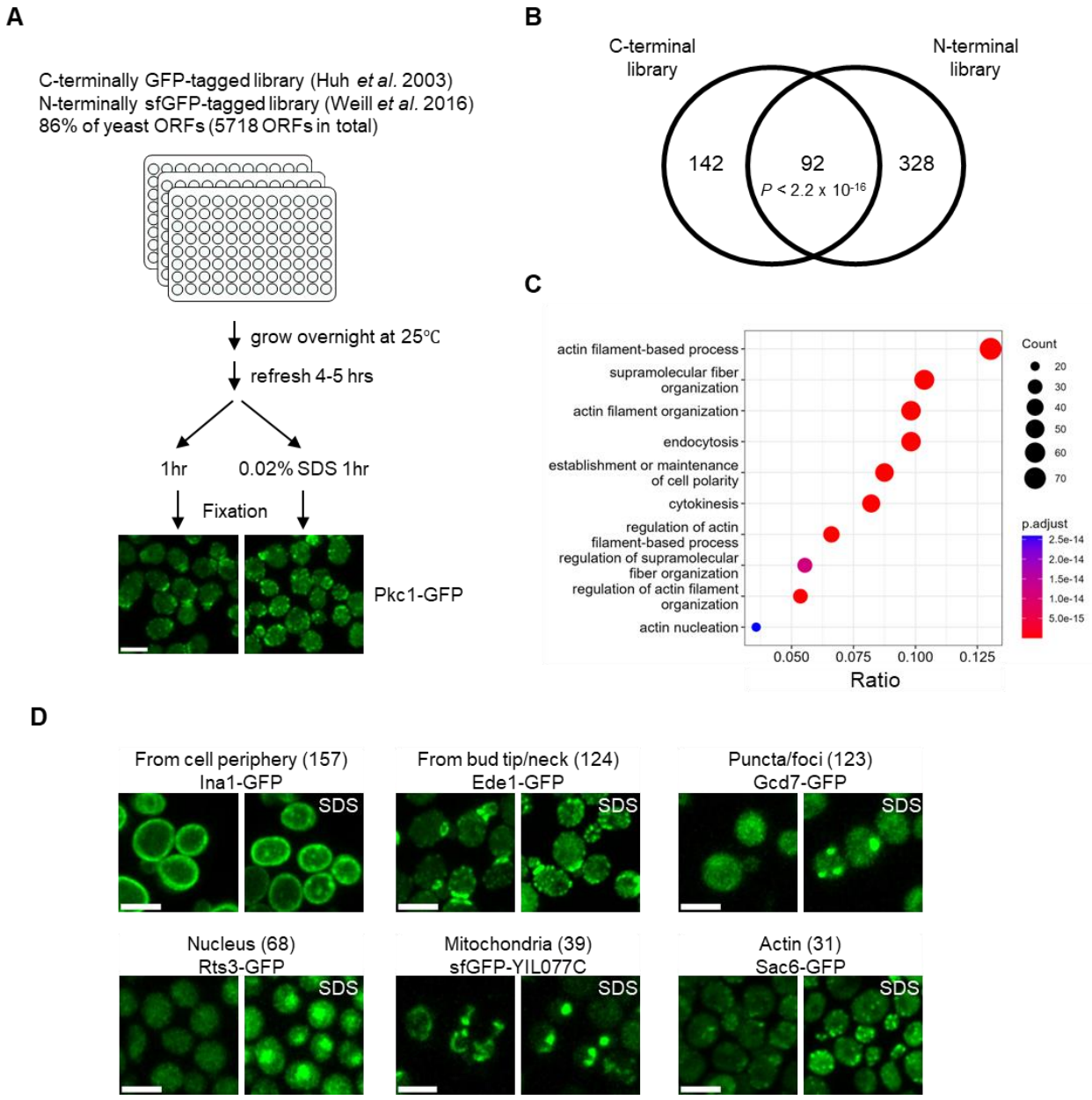

Fig. 1 Protein relocalization in response to SDS treatment.
(A) Schematic representation of screening methodology and images of Pkc1-GFP with or without 0.02 % SDS treatment were shown. Scale bar, 5 μm. **(B)** Overlap of screening hits of C- and N-terminal libraries. P value for the significance of the overlap is indicated. Fisher's exact test was performed. **(C)** GO analysis of biological processes for the screening hits. Successfully observed proteins were used as the background protein sets. **(D)** Screening hits for six relocalization classes and the images of representative proteins in each class were shown. Numbers in parentheses indicate the number of proteins in the class. Scale bar, 2 μm.

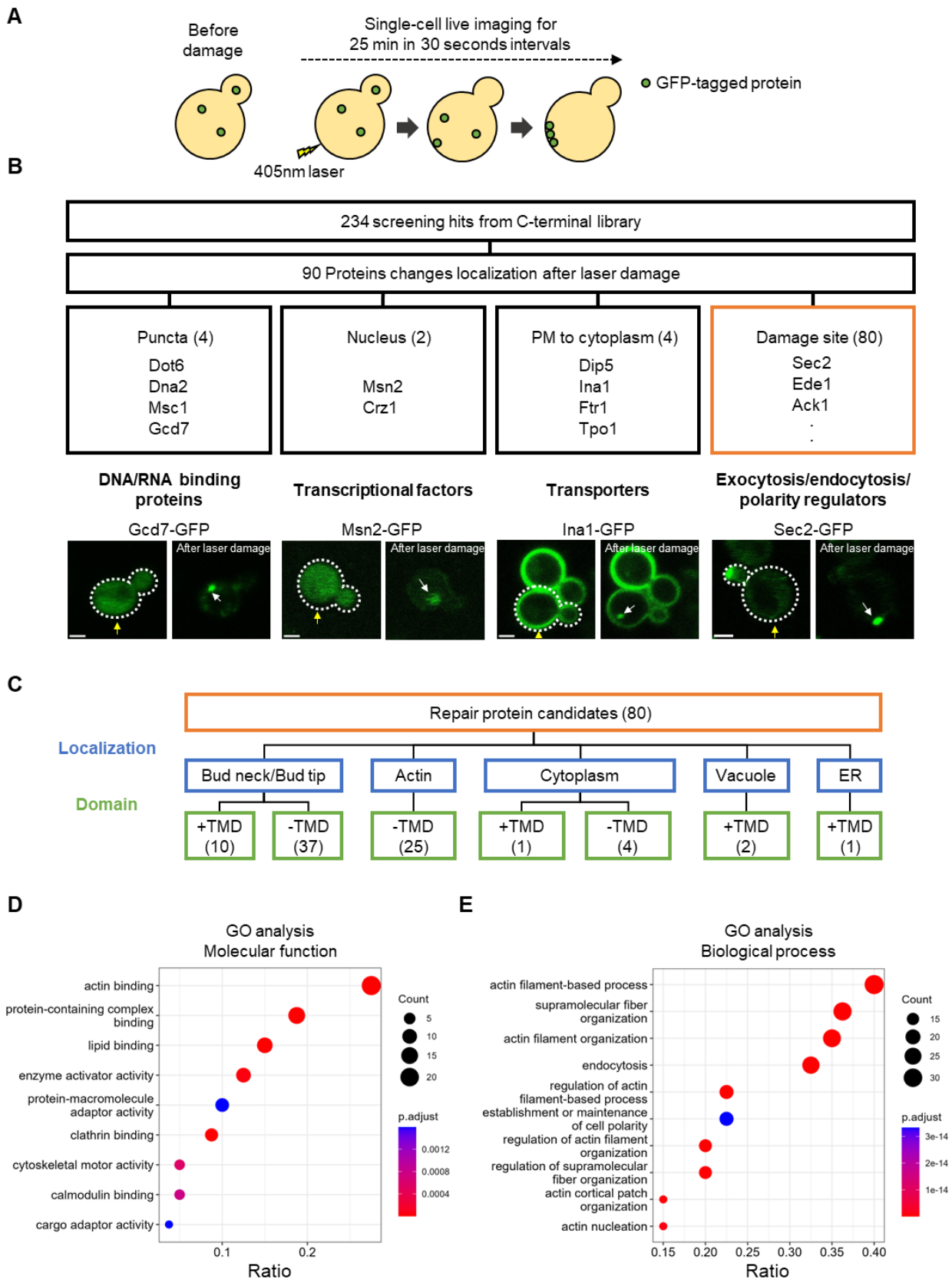

Fig. 2 Laser damage assays identified 80 repair protein candidates.
(A) Schematic representation of screening methodology. Cells were imaged for 25 min in 30-second intervals after 405 nm laser damage. **(B)** 90 proteins change localization after laser damage. The classification of the repair protein candidates based on their localization changes,

representative proteins, and representative biological processes in each category are shown. Scale bar, 2 μm. Yellow arrows show the damage site. White arrows show the recruitment of fluorescence signals. **(C)** Classification of repair protein candidates based on subcellular localization and domain. TMD+ represents the proteins that have transmembrane domains. The existence of transmembrane domains was predicted by TMHMM (*62*) **(D)** GO analysis of molecular functions for the repair protein candidates. The proteins whose localization changes in response to SDS treatment were used as the background protein sets. **(E)** GO analysis of biological processes for the repair protein candidates. The proteins whose localization changes in response to SDS treatment were used as the background protein sets.

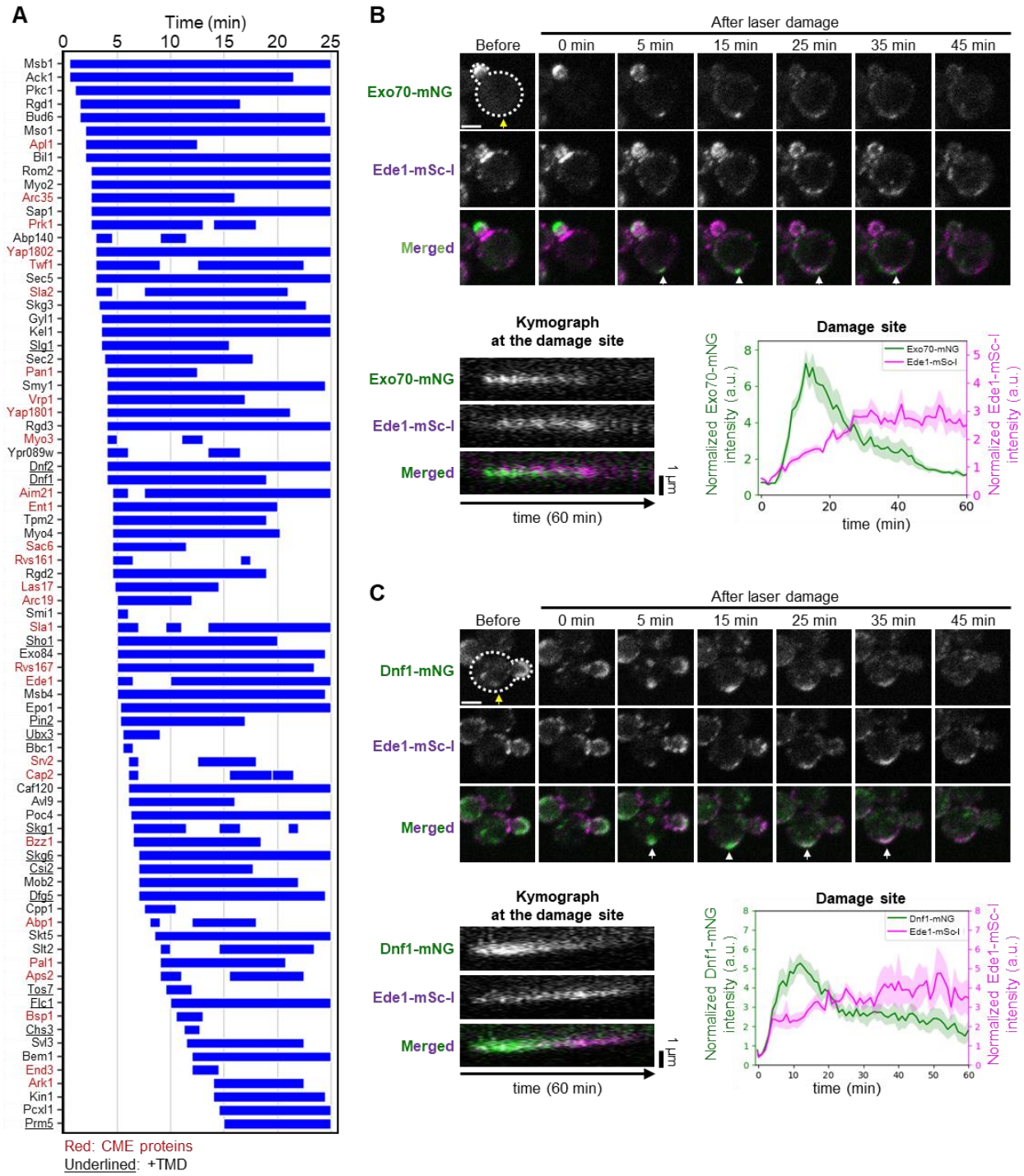

Fig. 3 The order of repair protein recruitments.
(A) The bar graph starts from the accumulation time to the dispersion time. See Material and Methods for details. **(B)** Representative images, kymograph at the damage site, and fluorescence intensity at the damage site of Exo70-mNG (Green) and Ede1-mSc-I (purple). Lines and shaded regions are the mean and the standard error of the mean. n = 10 cells. Yellow arrows show the damage site. White arrows show the coaccumulation of Exo70-mNG and Ede1-mSc-I at the damage site. **(C)** Representative images, kymograph at the damage site, and fluorescence intensity at the damage site of Dnf1-mNG (Green) and Ede1-mSc-I (purple). Lines and shaded regions are the mean and the standard error of the mean. n = 9 cells. Yellow arrows show the damage site. White arrows show the coaccumulation of Dnf1-mNG and Ede1-mSc-I.

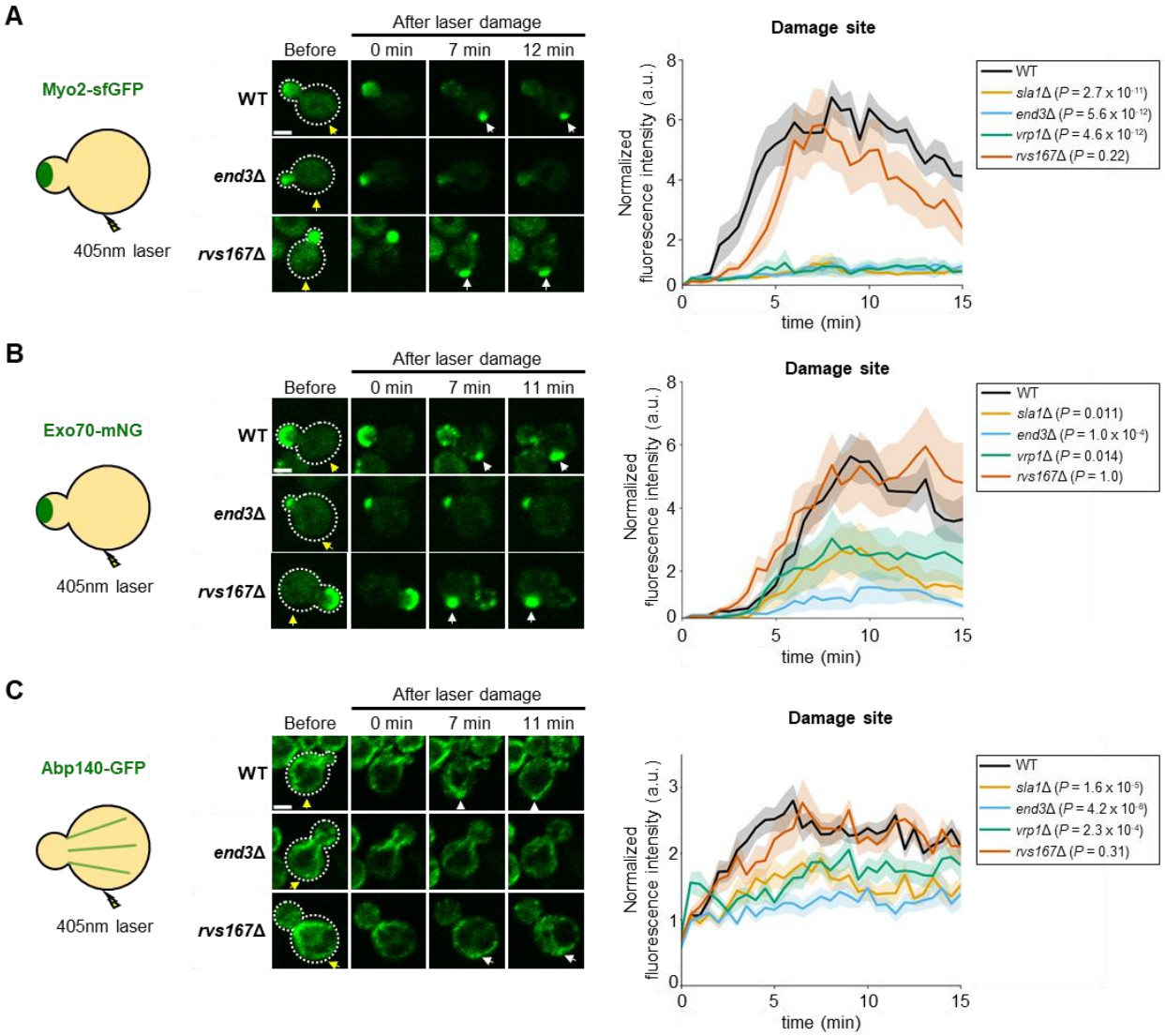

Fig. 4 CME proteins are required for polarized exocytosis and actin cable organization at the damage site.

(A) Experimental design, representative images of Myo2-sfGFP, and the quantification of fluorescence intensity at the damage site. n = 13 for WT, n = 12 for *end3*Δ, *sla1*Δ, *vrp1*Δ, and *rvs167*Δ **(B)** Experimental design, representative images of Exo70-mNG, and the quantification of fluorescence intensity at the damage site. n = 18 for WT, n = 12 for *end3*Δ, *sla1*Δ, and *rvs167*Δ n = 14 for *vrp1*Δ. **(C)** Experimental design, representative images of Abp140-GFP, and the quantification of fluorescence intensity at the damage site. n = 25 for WT, n = 14 for *end3*Δ, *sla1*Δ, and *vrp1*Δ, n = 15 for *rvs167*Δ. Lines and shaded regions are the mean and standard error of the mean. Maximum fluorescence intensity was compared between WT and mutants using Dunnett's multiple comparison test. Yellow arrows show the damage site. White arrows show the recruitment of fluorescence signals.

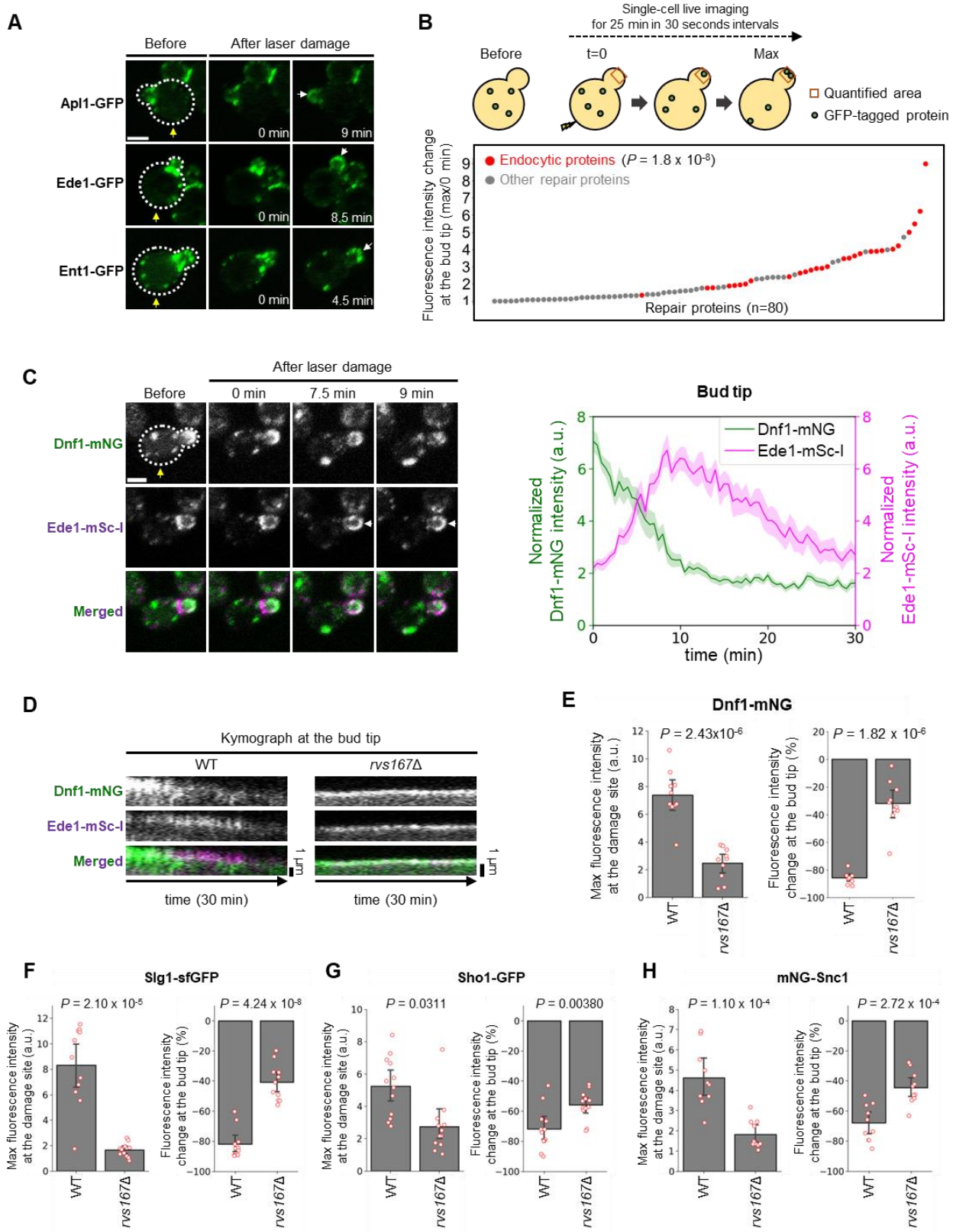

Fig. 5 CME at the bud tip directs repair proteins with TMDs to the damage site. **(A)** Representative images of Apl1-GFP, Ede1-GFP, and Ent1-GFP. **(B)** The ratio of maximum normalized fluorescence intensity at the bud tip to the normalized fluorescence intensity at 0 min at the bud tip for all repair protein candidates. Red: CME proteins. The list of CME proteins is adapted from (53). The *P* value was calculated by the two-sided Mann–Whitney U test. **(C)** Representative images and the normalized fluorescence intensity at the bud tip of Dnf1-mNG and

Ede1-mSc-I. **(D)** Kymograph of Dnf1-mNG and Ede1-mSc-I at the bud tip in WT and *rvs167*Δ. n = 10 cells. **(E)-(H)** Max fluorescence intensity at the damage site and fluorescence intensity changes at the bud tip in WT and *rvs167*Δ. n = 10 cells for Dnf1-mNG. n = 11 cells for Slg1-sfGFP. n = 12 cells for Sho1-GFP. n = 10 cells for mNG-Snc1. Welch's t-test was performed. Yellow arrows show the damage site. White arrows show the recruitment of fluorescence signals.

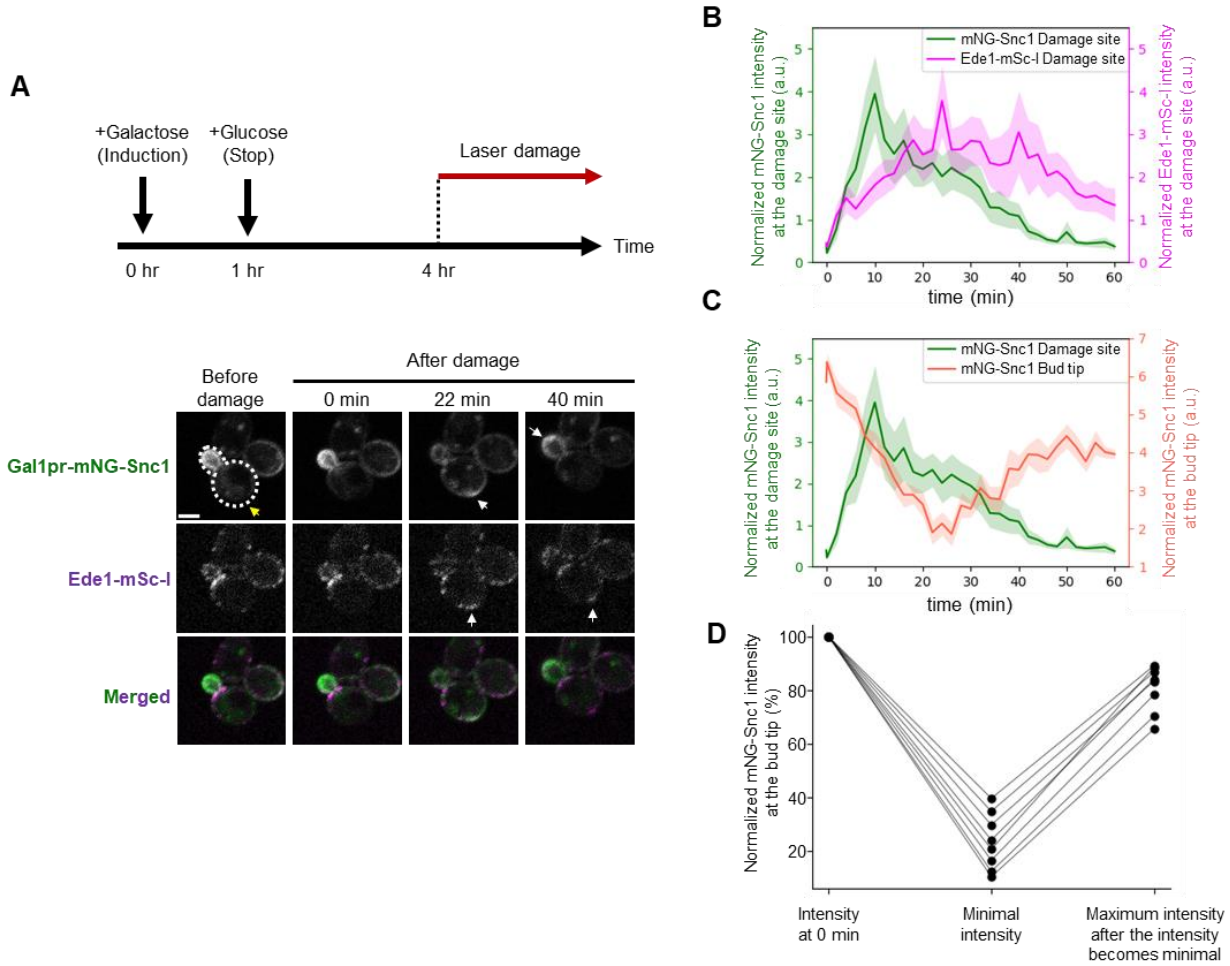

Fig. 6 mNG-Snc1 is recovered from the damage site to the bud tip after PM repair. **(A)** Schematic of transient expression induction of mNG-Snc1 by Gal1 promoter and representative images of mNG-Snc1 and Ede1-mSc-I. After transcription activation of the Gal1 promoter by adding 3% galactose, we stop the expression by transferring cells to glucose media. The cells were incubated for at least 3 hours before the laser damage assay. Yellow arrows show the damage site. White arrows showed the recruitment of fluorescence signals. **(B)** Quantification of mNG-Snc1 (Green) and Ede1-mSc-I (purple) at the damage site. **(C)** Quantification of mNG-Snc1 at the bud tip (Green) and at the damage site (tomato). **(D)** The changes of normalized mNG-Snc1 signal at the bud tip. n = 8 cells.

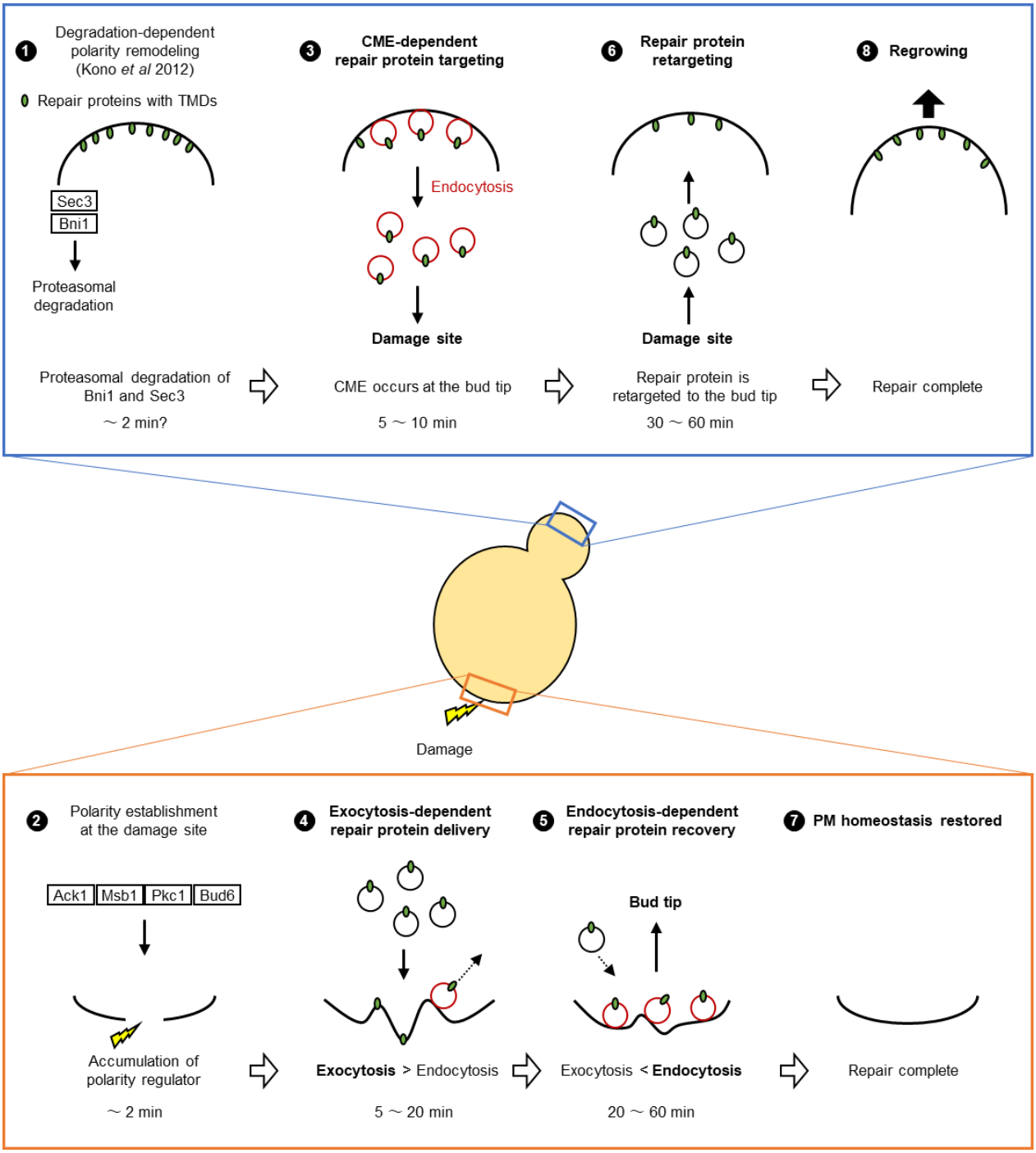

Fig. 7 Spatiotemporal PM damage responses and the hypothetical model of CME-dependent PM restructuring in budding yeast.

We showed the spatiotemporal PM damage responses in budding yeast. First, the degradation of Sec3 and Bni1 resolved the polarity competition between the bud tip and the damage site (*26*). Within 10 min after laser damage, CME directs repair proteins with TMDs to the damage site from the bud tip. At the damage site, exocytosis and CME simultaneously occur, with exocytosis predominating approximately within 20 min and with CME predominating approximately 20 min after laser damage. CME targets repair proteins with TMDs from the bud tip to the damage site. The endocytosed PM proteins are retargeted to the bud tip again after the PM repair is finished. The retargeted PM proteins may be involved in the resumption of cell growth after PM repair. The numbers represent the temporal order of events.